Geochimica et Cosmochimica Acta xxx (xxxx) xxx

Contents lists available at ScienceDirect

Geochimica et Cosmochimica Acta

journal homepage: www.elsevier.com/locate/gca

Selenium isotope constraints on sediment–oceanic crust interaction during slab deserpentinization

Juan Muñoz-Alfaro [a,*], Stephan König [a,b], Claudio Marchesi [c,d], Romain Tilhac [a,e], María Isabel Varas-Reus [b,f], José Alberto Padrón-Navarta [a], Vicente López Sánchez-Vizcaíno [g], Ronny Schoenberg [b], Carlos J. Garrido [a,*]

[a] Instituto Andaluz de Ciencias de la Tierra (IACT–CSIC), CSIC, 18100 Armilla, Granada, Spain
[b] Department of Geosciences, University of Tuebingen 72076 Tuebingen, Germany
[c] Departamento de Mineralogía y Petrología, Universidad de Granada 18002 Granada, Spain
[d] Raw Materials, Human and Environmental Health, Universidad de Granada, Associated Unit of the CSIC by the IACT-CSIC, 18100 Armilla, Granada, Spain
[e] Géosciences Montpellier, Université de Montpellier 34095 Montpellier, France
[f] Department of Geology (FCFM), Universidad de Chile, 8370458 Santiago, Chile
[g] Departamento de Geología, CEACTEMA, Universidad de Jaén 23700 Linares, Jaén, Spain

ARTICLE INFO

Associate editor: Julie Prytulak

Keywords:
Selenium isotopes
Serpentinite dehydration
Cerro del Almirez
Slab fluids
Arc volcanism

ABSTRACT

Arc magmas acquire their subduction-component signature through mantle-wedge metasomatism by slab-derived fluids and melts sourced in variable proportions from altered oceanic crust (AOC) and metasediments. At subarc depths, deserpentinization of slab mantle promotes this transfer by releasing large volumes of fluids that mobilize AOC- and sediment-derived components into the mantle-wedge source of arc volcanism. To constrain subarc fluid–rock interactions during slab deserpentinization, we present new selenium (Se) isotope data for rocks from the Cerro del Almirez ultramafic massif (Nevado–Filábride Complex, Betic Cordillera, southern Spain) formed in a subarc paleo-subduction setting. We report Se isotopes, radiogenic strontium (Sr) isotopes, and fluid-mobile element concentrations in metaserpentinites (antigorite-serpentinite), their subarc dehydration products (chlorite-harzburgite), interbedded metarodingites, and associated metasediments.

Relative to the primitive mantle ($\delta^{82/76}$Se = − 0.03 ± 0.07‰), metaserpentinites have heavier Se isotope compositions (with $\delta^{82/76}$Se ranging from − 0.04 to + 0.99‰), whereas metaharzburgites are isotopically lighter ($\delta^{82/76}$Se between − 0.80 and − 0.01‰). The lower $\delta^{82/76}$Se values of metaharzburgites relative to metaserpentinites and primitive mantle cannot be attributed to magmatic inheritance, as magmatic processes do not fractionate Se isotopes. Similarly, variations in seafloor serpentinization degrees cannot account for the sharp isotopic shift observed. Decreasing $\delta^{82/76}$Se with higher fluid-mobile element-to-Ce ratios and lower $^{87}Sr/^{86}Sr$ in metaharzburgites indicate equilibration with fluids derived from a mixed metasedimentary–AOC source during slab deserpentinization. To evaluate the relative roles of sediment-derived fluid infiltration and reaction with AOC within a deserpentinizing slab, we developed an open-system dehydration numerical model. The model indicates that open-system dehydration of a heterogeneous slab including metaserpentinites, AOC and metasediments produces fluids with AOC-like unradiogenic $^{87}Sr/^{86}Sr$, and sediment-like light Se isotope compositions, thereby accounting for the trends observed in Cerro del Almirez metaharzburgites. These results imply that intra-slab reactive infiltration of sediment-derived fluids during deserpentinization of an AOC-bearing slab modulates the relative sediment–AOC contributions to subduction-zone fluids that flux the mantle-wedge source of primitive arc magmas.

* Corresponding authors.
E-mail addresses: juan13geo@gmail.com (J. Muñoz-Alfaro), carlos.garrido@csic.es (C.J. Garrido).

https://doi.org/10.1016/j.gca.2026.07.049
Received 16 January 2026; Accepted 31 July 2026
Available online 11 August 2026

1. Introduction

Subduction zones are key geological settings for the recycling of water and other volatiles from the Earth's surface into the deep mantle (Cerpa et al., 2022; Hirschmann, 2023). As the oceanic plate descends, increasing pressure (P) and temperature (T) cause the metamorphic breakdown of hydrous minerals from different slab lithologies, most notably serpentine, generating aqueous-rich fluids that metasomatize the mantle-wedge source of primitive arc basalts (e.g., Schmidt and Poli, 2014). This cascade of slab metamorphic devolatilization reactions triggers fluid-mediated chemical reactions at different slab depths. At subarc depths, these fluids are primarily released from antigorite breakdown, generating large fluid fluxes that subsequently interact with surrounding slab and slab-interface lithologies, including metasedimentary rocks, altered oceanic crust, and mélange-zone rocks. These fluids and/or melts migrate into the mantle wedge, imparting the distinctive "subduction component" signature to arc magmas (Bebout, 2007, 2014).

The subduction component of oceanic arc magmatism is typified by enrichment in fluid-mobile elements (FME, e.g., Cs, Ba, Sr, and Pb) and by radiogenic and stable isotope signatures reflecting recycled slab lithologies. These geochemical signatures are usually ascribed to the variable contribution of slab-derived fluids and/or melts from three end-member slab lithologies: namely, sediments, altered oceanic crust (AOC), and, to some extent, serpentinite. Terrigenous sediments may contribute substantial enrichments in FME and high $^{87}Sr/^{86}Sr$ and low $^{143}Nd/^{144}Nd$ ratios, reflecting their continental crust provenance. The AOC imparts an intermediate signature, showing modest enrichments in FME relative to unaltered MORB and slightly radiogenic Sr isotope ratios due to seawater alteration during mid-ocean ridge hydrothermal circulation. Serpentinite dehydration yields volatile-rich aqueous fluids (Alt et al., 2013; Halama et al., 2014; Kendrick et al., 2018; Scambelluri et al., 2019) with distinctive isotopically heavy boron and light iron (e.g., Scambelluri and Tonarini, 2012; Harvey et al., 2014; Debret et al., 2016; Chen et al., 2023). Crucially, the efficiency of this elemental and isotopic transfer depends not only on the slab source components but also on the physical nature of the transporting phase. Element behaviour and solubility vary between dilute aqueous fluids, hydrous silicate melts, brines and supercritical liquids generated at high pressures, which can modify the slab-derived geochemical signature (Kessel et al., 2005). Together, these contributions yield the characteristic trace element patterns, such as elevated ratios of large-ion lithophile elements to high-field-strength elements, and isotopic features observed in arc magmas (Elliott, 2003; Bebout, 2014; Bebout and Penniston-Dorland, 2016).

Traditionally, the relative contributions of sediment- and AOC-derived slab components to arc magmatism have been modelled as variable mixtures of slab-derived fluid end members (Elliott, 2003; Plank, 2014; Turner and Langmuir, 2024). However, the geochemical signature of slab fluids is likely shaped during intra-slab fluid–rock reactions across different slab lithologies during transient pulses associated with metamorphic devolatilization reactions (Connolly, 1997; Schmidt and Poli, 1998; Zack and John, 2007; John et al., 2008, 2012; Padrón-Navarta et al., 2010a; Plümper et al., 2017). A growing body of work indicates that the main source of subarc slab-derived fluids is high-pressure deserpentinization of the slab hydrated mantle lithosphere (e.g., Ulmer and Trommsdorff, 1995; Schmidt and Poli, 1998; Scambelluri et al., 2019). At depth, deserpentinization fluids interact with fluid-saturated eclogite and metasedimentary rocks (e.g., John et al., 2008; Chen et al., 2019; Ague et al., 2022; Padrón-Navarta et al., 2023). However, the extent to which fluids from different slab lithologies interact with subarc deserpentinization fluids, and how these interactions control the geochemical and isotopic character of the subduction component, remains poorly constrained (e.g., Zack and John, 2007; John et al., 2008).

Investigations of exhumed mélange zones reveal the inherent complexity of these interactions, but they typically provide insight into shallower forearc processes. Exhumed eclogite-facies metamorphic terranes, by contrast, offer a snapshot of these dynamics and can serve as archives for deciphering the processes that ultimately shape the geochemical signature of slab-derived fluids (Bebout, 2007). Here, we examine metaserpentinites and their deserpentinization products (metaharzburgites) from the Cerro del Almirez ultramafic massif (Betic Cordillera, southern Spain). This eclogite-facies paleo-subduction terrane preserves a well-exposed deserpentinization front in serpentinized oceanic lithosphere that contains mafic intrusions transformed into rodingites during seafloor hydrothermal metasomatism (Trommsdorff et al., 1998; Padrón-Navarta et al., 2011; Laborda-López et al., 2018). Recent studies have shown that antigorite dehydration was coeval with the infiltration of metasediment-derived fluids (Garrido et al., 2005; Marchesi et al., 2013; Harvey et al., 2014; Kendrick et al., 2018; Debret et al., 2021; Padrón-Navarta et al., 2023; Xiong et al., 2023). The Cerro del Almirez massif, therefore, provides an exceptional opportunity to examine how deserpentinization fluids interacted with co-subducted sediments and AOC. In this framework, radiogenic strontium (Sr) and stable selenium (Se) isotopes act as complementary component tracers. While $^{87}Sr/^{86}Sr$ signatures fingerprint the bulk source lithologies, $\delta^{82/76}Se$ compositions trace both the distinct inherited redox environments of those source components and redox-driven fluid processes. By analyzing these complementary isotope compositions alongside FME systematics in metaserpentinites and metaharzburgites, we constrain the interaction and evolution of slab-derived fluids during subarc deserpentinization. These data clarify how slab components mix and react during fluid transfer to the mantle wedge, and how this transfer contributes to the subduction-component signature of arc magmatism.

2. Geological setting and sample selection

The Cerro del Almirez (CdA) ultramafic massif (Betic Cordillera, South Spain), covering *c.* 2.3 km^2, is one of the metaultramafic massifs within the Nevado-Filábride Complex (NFC) (Trommsdorff et al., 1998; Puga et al., 1999), the deepest metamorphic unit of the internal zones of the Betic Cordillera (SE Spain) (Fig. 1a) (Jabaloy-Sánchez et al., 2019). The massif consists of a section of mantle from the Jurassic SE Iberian hyperextended continental margin that underwent seafloor serpentinization prior to subduction during the Alpine orogeny, reached eclogite-facies conditions, and was subsequently exhumed (Puga et al., 1999; Dilissen et al., 2018; Gómez-Pugnaire et al., 2019).

The CdA massif (Fig. 1b) consists of foliated antigorite-serpentinite (Atg-serpentinite: Atg + Ol + Chl + Mag + Ilm ± Di ± Tr ± Ti-Chu; mineral abbreviations follow Whitney and Evans, 2010) overlying unfoliated chlorite-harzburgite (Chl-harzburgite: Ol + Opx + Chl + Mag + Ilm ± Ti-Hem ± Tr ± Ti-Chu). Chl-harzburgites, formed at ~ 650 °C and 1.6–1.9 GPa, exhibit either granofels or spinifex-like textures in intercalated lenses, some of which are locally recrystallized along grain-size reduction zones (Trommsdorff et al., 1998; Padrón-Navarta et al., 2010a, 2011, 2015; Dilissen et al., 2018). The Atg-serpentinite to Chl-harzburgite transition has been interpreted as a dehydration isograd (Trommsdorff et al., 1998; Padrón-Navarta et al., 2010b, 2011), a reaction front driven by external fluid infiltration during high-pressure deserpentinization from a common fully serpentinized protolith (Padrón-Navarta et al., 2023), or as a metamorphic boundary controlled by hydration and redox gradients inherited from a pre-subduction oceanic serpentinization front (e.g., Bretscher et al., 2018; Vieira Duarte et al., 2021; Pettke and Bretscher, 2022). Metarodingite boudins, up to 2 m thick, also occur with chlorite and hybrid-rock blackwalls, and are enclosed in both metaserpentinite and metaharzburgite; they record a history from seafloor rodingitization to high-pressure antigorite dehydration conditions (Laborda-López et al., 2018, 2020). These boudins, originally formed by seafloor rodingitization of mafic intrusions in the oceanic lithosphere, underwent successive

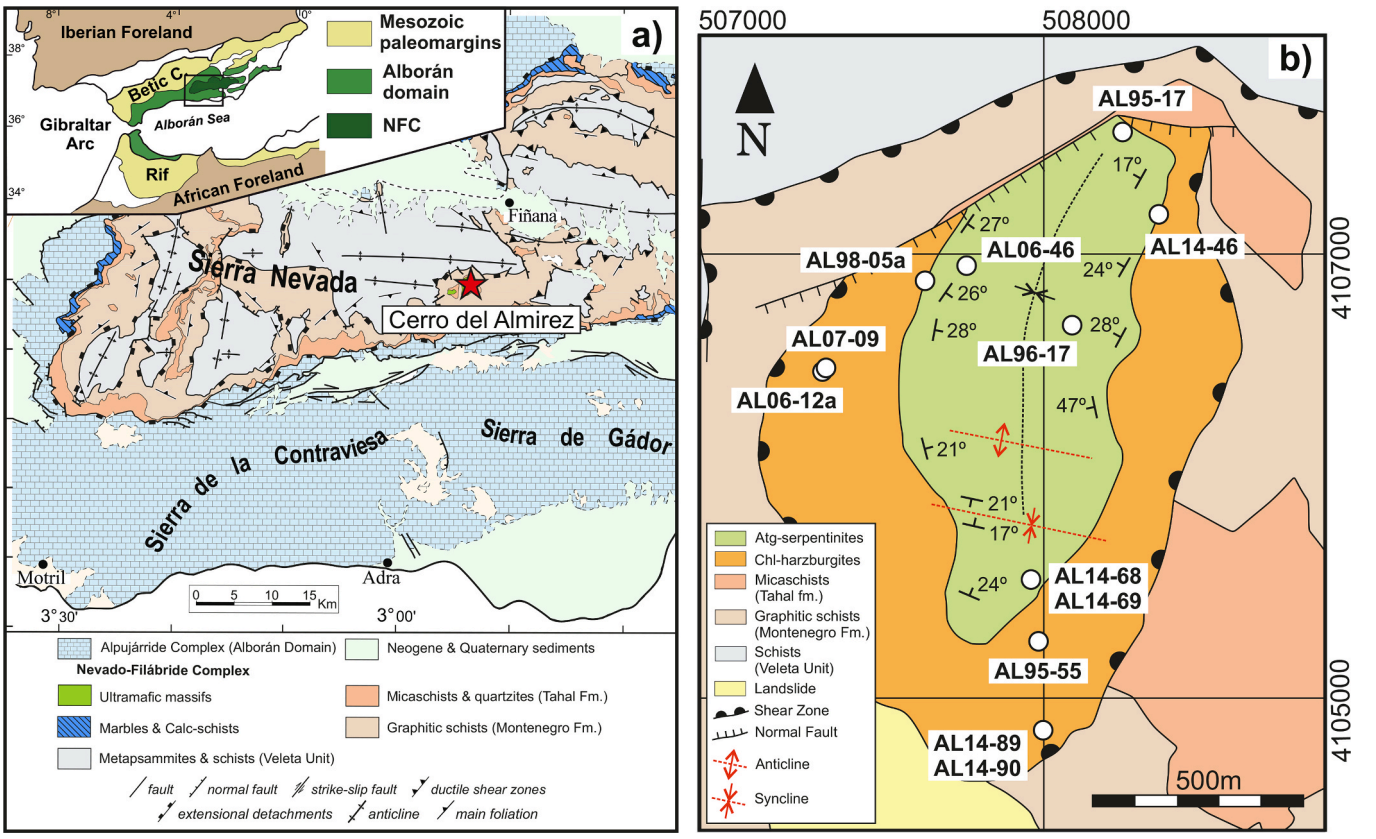

Fig. 1. (a) Geological map of the Nevado-Filábride Complex in the Betic Cordillera, South Spain (upper left inset), showing the location of Cerro del Almirez (modified from Martínez-Martínez et al., 2002, and Jabaloy-Sánchez et al., 2015). (b) Simplified geological map of Cerro del Almirez showing the location of the studied Atg-serpentinites and Chl-harzburgites.

metasomatic transformations during Alpine subduction.

For this study, we analyzed seven Atg-serpentinites and six Chl-harzburgites, including four granofels-textured and two spinifex-textured samples. Most samples were collected from the Almirez peak area (Fig. 1b), with additional samples from the nearby Prado Mocho area. To evaluate the potential contribution of fluids from metarodingites and co-subducted metasedimentary rocks, we also analyzed two metarodingites and one Nevado-Filábride garnet micaschist. All samples have been previously characterized in detail for their petrology and elemental geochemistry, forming a well-documented dataset for this investigation (e.g., Garrido et al., 2005; Alt et al., 2012; Marchesi et al., 2013; Harvey et al., 2014; Laborda-López et al., 2018, 2020; Debret et al., 2021). Sample descriptions, locations, and petrographic summaries are provided in Table S1 (Supplementary Data 1).

3. Analytical methods

Details about the analytical procedures can be found in the Supplementary Information (section A). Given the low Se concentrations in the samples (as low as 7 ng·g^{-1}), 450 mg of sample powder was weighed into pre-cleaned PFA vials. A ^{74}Se–^{77}Se double spike solution was added to achieve a Se_{sample}/Se_{spike} ratio of ~ 1, based on Se concentrations previously determined by hydride generation ICP quadrupole mass spectrometry (ICP-QMS). Sample powders were digested on a hot plate following the methods of Yierpan et al. (2018) and Kurzawa et al. (2017). Briefly, sample powders were subjected to a multi-step hot-plate digestion using a concentrated HNO_3–HF mixture (1:5 ratio) at 85 °C for 24 h in PFA vials. To eliminate fluorides, solutions were evaporated to dryness at 65 °C, redissolved in 6 M HCl at 130 °C for 48 h, and dried twice with 1 mL of 11 M HCl at 65 °C. Samples were finally taken up in 5 mL of 4 M HCl and heated overnight at 65 °C to ensure the total reduction of Se^{6+} to Se^{4+} prior to chromatography. Selenium was separated from Fe using 7 mL Bio-Rad AG 1-X8© anion resin (100–200 mesh) and from other matrix elements with 7 mL Bio-Rad AG 50 W-X8© cation resin (100–200 mesh), following the method of Yierpan et al. (2018). Additionally, some samples with high Ge contents required an extra chromatography with 7 mL Bio-Rad AG 1-X8© anion resin (100–200 mesh), where Se was separated from Ge with 1 M HF, based on the method from Rouxel et al. (2006). The Se fraction was evaporated at 65 °C and redissolved in 1.1 mL of 2 M HCl for mass spectrometry. Selenium isotope analysis (reported as $\delta^{82/76}$Se, i.e., deviation of sample $^{82}Se/^{76}Se$ relative to reference solution NIST SRM 3149) was performed using a hydride generator connected to a Neptune XT (at IACT-CSIC, Granada, Spain) and Neptune Plus (at the University of Tuebingen, Germany) multi-collector inductively coupled plasma mass spectrometers (MC-ICP-MS). The external reproducibility of $\delta^{82/76}$Se is conservatively reported as ± 0.25‰ (2 s.d.), based on repeated analyses of the inter-laboratory standard solution MH-495 (15 ng·mL^{-1} Se) and Chl-harzburgite AL14-89, which yielded average $\delta^{82/76}$Se values of − 3.26 ± 0.23‰ (2 s.d., n = 22) and − 0.01 ± 0.25‰ (2 s.d., n = 5), respectively. Analyses of the rock reference material BCR-2 and the in-house standard Navajún pyrite (König et al., 2019) yielded $\delta^{82/76}$Se values of + 0.21 ± 0.07‰ (2 s.d., n = 3) and − 2.74 ± 0.17‰ (2 s.d., n = 2), respectively, both consistent with previously published values (Kurzawa et al., 2019; König et al., 2021; Yierpan et al., 2021). Total procedural blanks, encompassing the entire chemical processing from sample dissolution through all ion-exchange chromatography steps, were consistently below the instrumental background level (< 40 pg of total Se). Given the lowest sample concentration (7 ng·g^{-1} whole rock Se, repeatedly processed to yield ~ 7 ng of total Se in a 1 mL final solution), this potential maximum blank contribution would account for less than 0.6% of the total Se mass processed, which is negligible.

For strontium isotope analysis, ca. 100 mg of sample powder was digested following a protocol adapted from Weis et al. (2006). Briefly, sample powders were digested in PFA vials using a 14 M HNO_3–24 M HF mixture at 120 °C for 72 h. Following fluoride removal, the residue was taken up in 1 mL of 2.5 M HCl and loaded onto columns packed with a 7 mL bed of Bio-Rad AG 50 W-X8© (200–400 mesh) cation resin following Kochergina et al. (2022). Strontium isotope ratios were measured on a Neptune XT MC-ICP-MS at IACT-CSIC with sample introduction via a cyclonic glass spray chamber in wet-plasma mode, following an instrumental setup and data treatment based on Yang et al. (2008) and Yang et al. (2014). The procedural blank was negligible (< 50 pg of total Sr). Age correction was performed by subtracting the radiogenic ^{87}Sr produced by ^{87}Rb decay since the time of peak subduction (15 Ma), using the sample Rb/Sr ratio and the decay constant of ^{87}Rb ($\lambda = 1.3972 \pm 0.0045 \times 10^{-11}$ yr^{-1}; Villa et al., 2015). Both measured and age-corrected (15 Ma) $^{87}Sr/^{86}Sr$ values are provided in Table S1. All figures in this study display age-corrected values.

4. Results

Trace element compositions for all samples were reported in previous studies (Garrido et al., 2005; Marchesi et al., 2013; Laborda-López et al., 2020). Table S2 (Supplementary Data 1) lists the subset of trace elements used in this study, together with $Fe^{3+}/\Sigma Fe$ and L.O.I. data.

Selenium and strontium concentrations and isotopic compositions of the studied samples are reported in Table S1 and illustrated in Fig. 2. Atg-serpentinites have Se concentrations ranging from 9 to 74 $ng{\cdot}g^{-1}$ and heavier Se isotope compositions ($\delta^{82/76}Se = -0.04$ to $+0.99$‰) compared to the primitive mantle ($\delta^{82/76}Se = -0.03 \pm 0.07$‰; Varas-Reus et al., 2019) (Fig. 2a). Except for one outlier, Atg-serpentinites display decreasing Se concentrations and increasing $\delta^{82/76}Se$ from primitive mantle values towards seawater-like values ($\delta^{82/76}Se = +0.41$ to $+1.59$‰; Chang et al., 2017) (Fig. 2a). In comparison, Chl-harzburgites exhibit a broader range of Se concentrations with higher maximum values (7 to 133 $ng{\cdot}g^{-1}$) and lower $\delta^{82/76}Se$ ($\delta^{82/76}Se = -0.80$ to -0.01‰) than Atg-serpentinites and the primitive mantle. Selenium concentrations in Chl-harzburgites show no correlation with $\delta^{82/76}Se$ (Fig. 2a). Strontium concentrations in Atg-serpentinites are 0.4–2.8 $\mu g{\cdot}g^{-1}$, with radiogenic isotope compositions ($^{87}Sr/^{86}Sr = 0.7091$–0.7136) relative to the primitive mantle ($^{87}Sr/^{86}Sr = 0.7045$; Zindler and Hart, 1986) (Fig. 2b). In contrast, Chl-harzburgites contain higher Sr concentrations (2.5–6.2 $\mu g{\cdot}g^{-1}$) and exhibit less radiogenic $^{87}Sr/^{86}Sr$ (0.7071–0.7092) than Atg-serpentinites. Within Chl-harzburgites, $\delta^{82/76}Se$ and $^{87}Sr/^{86}Sr$ show an inverse covariation with proxies of FME addition, such as Pb/Ce (Fig. 3a, d, S1a), Rb/Ce (Fig. 3b, e, S1b) and Cs/Ce (Fig. 3c, f, S1c). In the $^{87}Sr/^{86}Sr$ versus Sr/Ce plot (Fig. 2b), the Chl-harzburgite trend ranges from radiogenic values typical of Atg-serpentinites towards Jurassic-seawater values ($^{87}Sr/^{86}Sr = 0.7068$–0.7073; Wierzbowski et al., 2017). No systematic differences in Sr or Se isotopes are observed among Chl-harzburgite textural types (granofels vs spinifex), so they are treated as a single group hereafter.

Additionally, representative associated metarodingites and NFC metapelites were analyzed for comparison. The epidote-bearing metarodingite yields a remarkably heavy Se isotopic composition ($\delta^{82/76}Se = +2.09$‰; 22 $ng{\cdot}g^{-1}$) coupled with a relatively unradiogenic $^{87}Sr/^{86}Sr$ (0.7069; 1031 $\mu g{\cdot}g^{-1}$). In contrast, the pyralspite-bearing metarodingite records a lower $\delta^{82/76}Se$ value of + 0.80‰ (35 $ng{\cdot}g^{-1}$) and a similar $^{87}Sr/^{86}Sr$ of 0.7074 (238 $\mu g{\cdot}g^{-1}$). Finally, NFC metapelites exhibit Se concentrations ranging from 44 to 122 $ng{\cdot}g^{-1}$ (83 $ng{\cdot}g^{-1}$ on average, n = 3; Table S2) and 110 to 132 $\mu g{\cdot}g^{-1}$ Sr (116 $\mu g{\cdot}g^{-1}$ on average, n = 4, Table S2). A representative metapelite sample (AL96-12a) was analyzed for Se and Sr isotope compositions, yielding a distinctly light Se value ($\delta^{82/76}Se = -0.98$‰) and a highly radiogenic Sr signature ($^{87}Sr/^{86}Sr = 0.7246$).

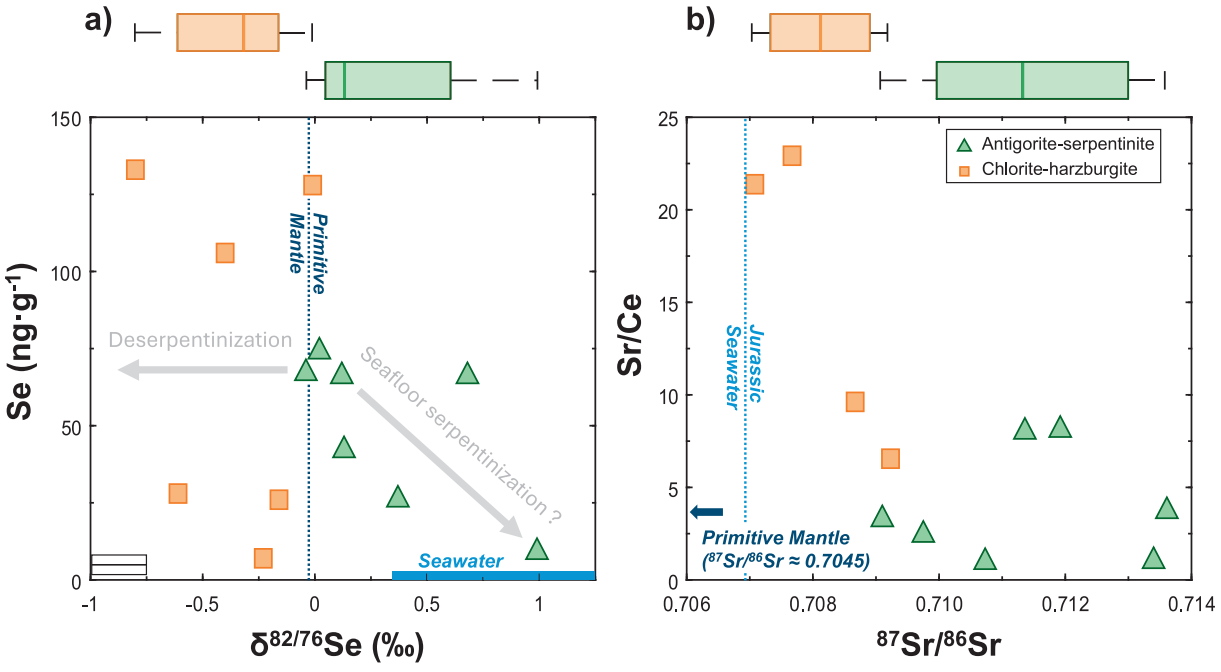

Fig. 2. Distribution of (a) $\delta^{82/76}Se$ vs. Se concentrations and (b) initial $^{87}Sr/^{86}Sr$ (back-calculated to 15 Ma) vs. Sr/Ce in Cerro del Almirez Chl-harzburgites (orange) and Atg-serpentinites (green). Box plots along the top axes illustrate the statistical distribution (median, interquartile range, and range) for each lithology. Except for one outlier, Atg-serpentinites display an inverse trend with increasing $\delta^{82/76}Se$ from the primitive mantle ($\delta^{82/76}Se = -0.03 \pm 0.07$‰; Varas-Reus et al., 2019) and approaching values characteristic of modern seawater ($\delta^{82/76}Se = +0.41$ to $+1.59$‰; Chang et al., 2017). In contrast, the lower $\delta^{82/76}Se$ values in Chl-harzburgites compared to Atg-serpentinites and the primitive mantle are interpreted to result from deserpentinization. Both lithologies exhibit more radiogenic Sr than the primitive mantle ($^{87}Sr/^{86}Sr \approx 0.7045$; Zindler and Hart, 1986), with Chl-harzburgites approaching less radiogenic Jurassic seawater values ($^{87}Sr/^{86}Sr$ minimum = 0.7068; Wierzbowski et al., 2017). The bottom left inset in (a) shows the 2SD for $\delta^{82/76}Se$ measurements. Analytical uncertainties for Sr isotope ratios are smaller than the symbol size.

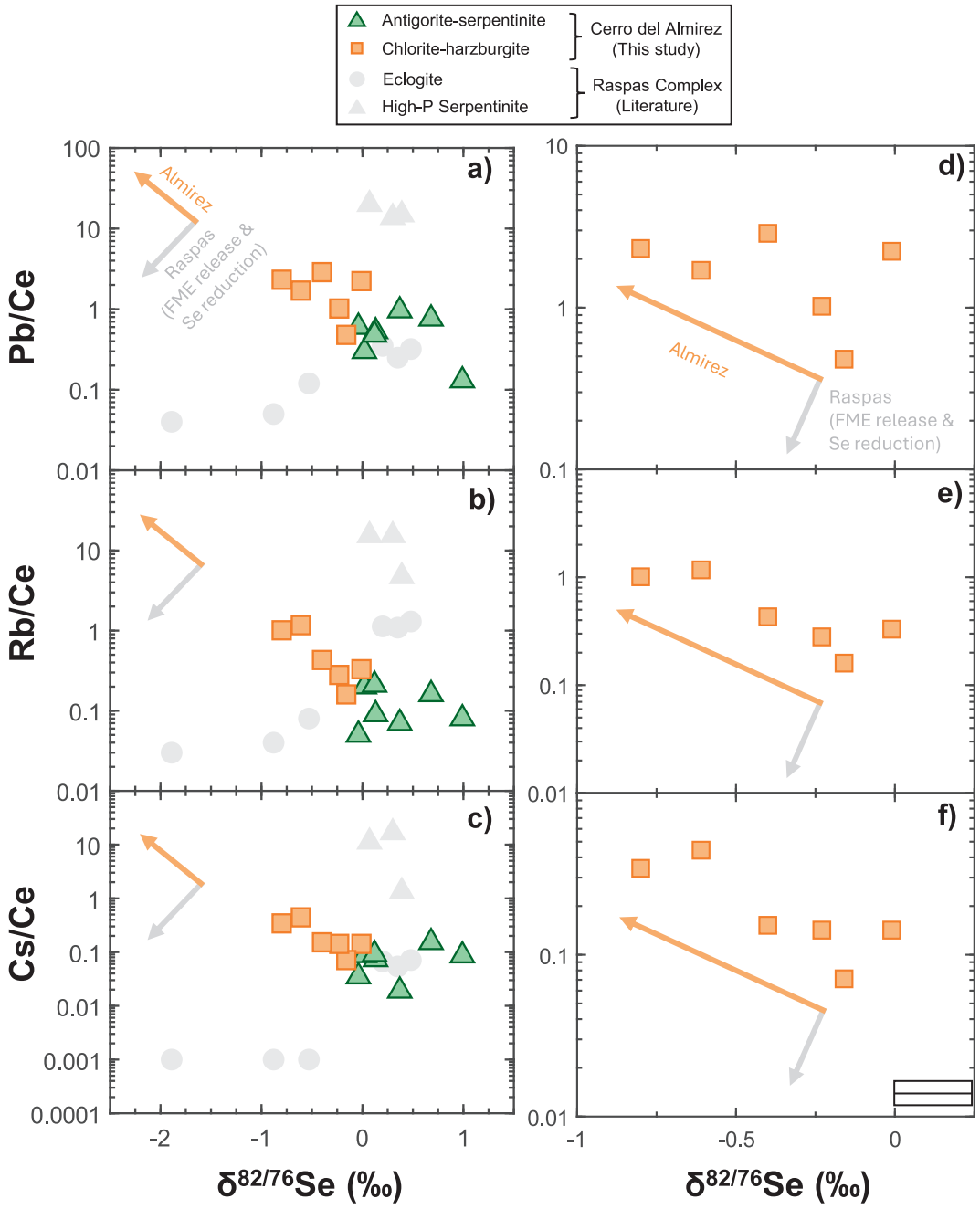

Fig. 3. Plots of $\delta^{82}/^{76}$Se vs. (a, d) Pb/Ce, (b, e) Rb/Ce, and (c, f) Cs/Ce ratios. Left panel (a–c): Overview comparing Cerro del Almirez samples (this study) with Raspas Complex eclogites and serpentinites (gray symbols; König et al., 2021). Arrows indicate divergent trends between the two complexes. Right panel (d–f): Zoomed view of the Cerro del Almirez Chl-harzburgites showing inverse trends between FME/Ce and $\delta^{82/76}$Se. Analytical uncertainties for $\delta^{82}/^{76}$Se are shown in the bottom right corner.

5. Discussion

5.1. Origin of the Se isotopic variability in Cerro del Almirez ultramafic rocks

The average Se isotope composition of Atg-serpentinites ($\delta^{82/76}$Se = +0.33 ± 0.29‰; 2sd/$\sqrt{n}$, n = 7) is statistically significantly heavier than that of Chl-harzburgites ($\delta^{82/76}$Se = − 0.37 ± 0.24‰; 2sd/$\sqrt{n}$, n = 6), which are notably lighter than the primitive mantle value (Varas-Reus et al., 2019) (Fig. 2a). The Se isotope signature of mantle peridotites is relatively homogeneous ($\delta^{82/76}$Se = − 0.03 ± 0.07‰; Varas-Reus et al., 2019), regardless of their degree of fertility. Given that Se isotopes appear not to be fractionated during partial melting and magmatic refertilization (Varas-Reus et al., 2019; Yierpan et al., 2020, 2021), a baseline further supported by the lack of correlation with fertility proxies such as Al_2O_3/SiO_2 (Fig. S2), the $\delta^{82/76}$Se variability in CdA metaultramafic rocks is better explained by processes other than magmatic heterogeneities in their oceanic mantle protoliths.

Heavier Se isotope compositions relative to the primitive mantle are a common feature of metaserpentinites from CdA (average $\delta^{82/76}$Se = +0.33 ± 0.29‰) and the Raspas Complex (average $\delta^{82/76}$Se = +0.25 ± 0.19‰; 2sd/$\sqrt{n}$, n = 3, König et al., 2021). In these ultramafic rocks, Se behaves as a strongly chalcophile element and is predominantly hosted within sulfides (e.g., pentlandite, pyrrhotite; Vieira Duarte et al., 2021) substituting for S^{2-}. Almirez Atg-serpentinites $\delta^{82/76}$Se show an inverse correlation with Se concentrations (Fig. 2a) consistent with the

replacement of magmatic sulfides by oxidized seawater characterized by elevated $\delta^{82/76}$Se and low Se concentrations (< 0.2 ng·g^{-1}; Chang et al., 2017; Stüeken, 2017). However, their Sr values are more radiogenic than coeval Jurassic seawater, a trend also documented in some abyssal serpentines (Snow et al., 1993; Hochscheid et al., 2022), suggesting contamination by detrital sediments. Although a robust $\delta^{82/76}$Se dataset currently lacks for abyssal serpentinites, we interpret that the heavy Se signature in CdA metaserpentinites may reflect seafloor serpentinization, forearc interaction with sediment-derived fluids, or the interplay of both. The distinctly lighter Se isotope values of Chl-harzburgites relative to metaserpentinites (Fig. 2), coupled with a systematic decrease in Loss on Ignition (LOI) and $Fe^{3+}/\Sigma Fe$ (Fig. 4), may be linked to the origin of the transition from Atg-serpentinite to Chl-harzburgite in CdA. Three interpretations exist for this transition: (i) a closed-system Atg-dehydration isograd ("intrinsic deserpentinization") (Trommsdorff et al., 1998; Padrón-Navarta et al., 2011); (ii) an open-system deserpentinization front modulated by infiltration of external fluids ("extrinsic deserpentinization") (Padrón-Navarta et al., 2023); or (iii) a metamorphic boundary controlled by hydration and redox gradients

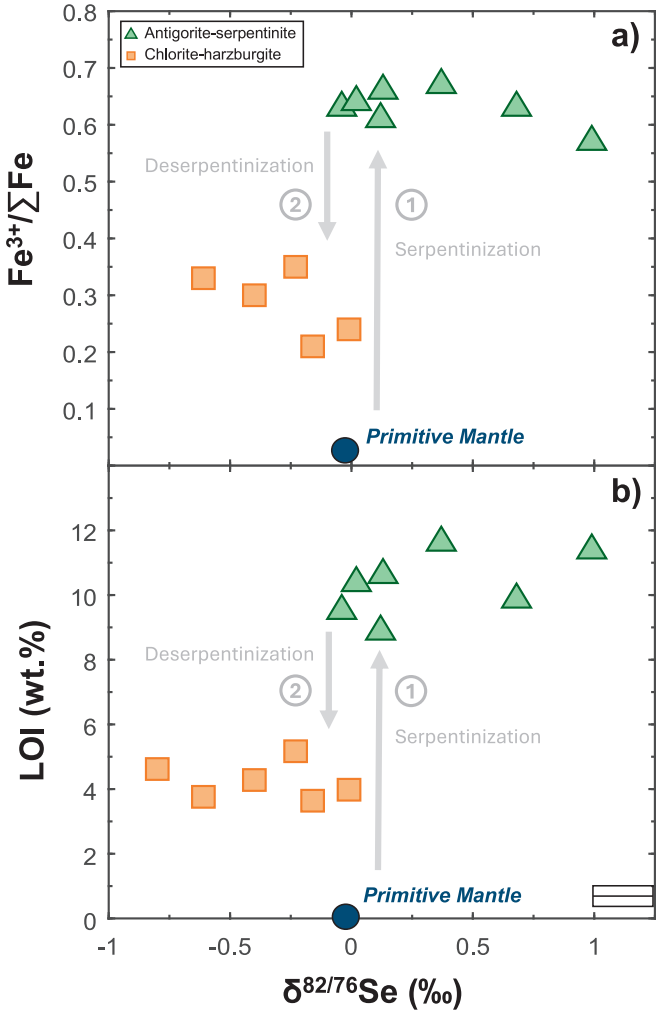

Fig. 4. Selenium isotope compositions of Cerro del Almirez Chl–harzburgites and Atg–serpentinites versus (a) $Fe^{3+}/\Sigma Fe$ ratio and (b) Loss on ignition (LOI; wt. %), respectively, as proxies of (a) oxidation and (b) hydration ($Fe^{3+}/\Sigma Fe$ and LOI data are provided in Table S2, Supplementary Material). Chl-harzburgites show statistically significantly lower $Fe^{3+}/\Sigma Fe$ ratios, LOI, and lighter Se values than Atg-serpentinites, where seafloor serpentinization promotes hydration and oxidation relative to primitive upper mantle values ($Fe^{3+}/\Sigma Fe$ = 0.023; O'Neill et al., 1993). Analytical uncertainties for $\delta^{82/76}$Se are shown in the bottom right corner.

inherited from a pre-subduction oceanic serpentinization front (Bretscher et al., 2018; Vieira Duarte et al., 2021; Pettke and Bretscher, 2022). Since pre-subduction variable oceanic serpentinization cannot account for the distinctly low $\delta^{82/76}$Se values in CdA Chl-harzburgites compared to the primitive mantle (Fig. 2a), these isotopic data support an origin via subarc high-P antigorite dehydration (i.e., scenarios i or ii). This deserpentinization-driven Se isotope variability is strongly supported by the robust inverse correlations between $\delta^{82/76}$Se and FME/Ce ratios, such as Cs/Ce, Pb/Ce, and Rb/Ce (Fig. 3). While these ratios during low-temperature seafloor alteration are affected by variable Ce mobility (Debret et al., 2024), the systematic covariation between FME concentrations and FME/Ce ratios observed in our sample suite (Fig. S3) is a diagnostic hallmark of subarc slab-fluid infiltration. Furthermore, these chemical variations are in excellent agreement with previously published large datasets for ultramafic rocks from the Cerro del Almirez massif (e.g., Marchesi et al., 2013; Laborda-López et al., 2020), confirming that our sample suite is representative of this locality. Likewise, the lack of correlation between FME/Ce and La/Yb ratios (Fig. S3) points to negligible fractionation of LREEs relative to heavy REEs (HREEs) during subarc slab metasomatism, further reinforcing the immobility of REEs during this process. The tight correlation between lighter $\delta^{82/76}$Se and elevated FME/Ce ratios firmly rules out any potential inheritance from a seafloor serpentinization stage, demonstrating that the observed isotopic shift was directly driven by metasomatism at subarc depths.

5.2. *Redox-driven fractionation of Se isotopes during slab dehydration*

Equilibrium selenium isotope fractionation is predominantly driven by changes in bond stiffness during redox reactions, where the heavy isotopes preferentially partition into the stronger, stiffer bonds of oxidized species (Se^{VI} or Se^{IV}), leaving the weaker bonds of reduced species (Se^0 or Se^{-II}) isotopically light (Johnson, 2004). Two distinct equilibrium pathways need to be considered at sub-arc temperatures. Under a reduced devolatilization pathway the solid-bound and fluid-bound Se species share the same valence and $\Delta^{82/76}$Se(sulfide–fluid) is essentially zero at ≥ 650 °C (Li and Liu, 2011; see section B in Supplementary Information, Supplementary Data 2 and Fig. S4), so no isotopic shift can be generated. Under an oxidized pathway the equilibrium fractionation between HSe^- and selenate (or selenite) is large even at sub-arc temperatures (ε ≈ +2.95‰ and + 1.64‰, respectively, at 650 °C; Li and Liu, 2011) and would in principle drive the residue toward lighter compositions upon selective removal of the isotopically heavy oxidized species. This equilibrium scenario is, however, not expected to operate in the natural setting: the oxidative mobilization of Se (−II) is kinetically controlled and induces negligible isotopic fractionation in practice (typically < 0.5‰; Johnson, 2004; Stüeken et al., 2015), so the equilibrium curves in Fig. S4 represent only theoretical upper bounds.

Independent of any theoretical scenario, the CdA dataset itself is incompatible with closed-system Rayleigh extraction. Chl-harzburgites are not depleted in Se relative to Atg-serpentinites (means of 71 and 50 ng·g^{-1}, respectively; Table S1), so the residue has not lost Se on average. Within the Chl-harzburgite group, $\delta^{82/76}$Se shows no correlation with Se concentration (r = − 0.18, n = 6): the isotopically lightest sample (AL07-09; $\delta^{82/76}$Se = − 0.80‰) contains 133 ng·g^{-1} and the isotopically heaviest one (AL14-89; $\delta^{82/76}$Se = − 0.01‰) contains 128 ng·g^{-1}, both well above the mean Atg-serpentinite value. In contrast, $\delta^{82/76}$Se covaries strongly with $^{87}Sr/^{86}Sr$ (r = +0.89) and with FME/Ce ratios (Figs. 3, 5). These observations require open-system addition of externally derived Se rather than *in situ* closed-system fractionation, as further developed in Sections 5.3 and 5.4.

The Raspas Complex (SW Ecuador) represents a paleo-subduction terrane that reached peak eclogite-facies conditions (~2.0 GPa, 600 °C, similar to CdA: ~1.8 GPa, 650 °C) and is primarily dominated by eclogites, metaserpentinites and pelitic schists. In this complex, subduction-related metamorphic dehydration of oceanic crust to

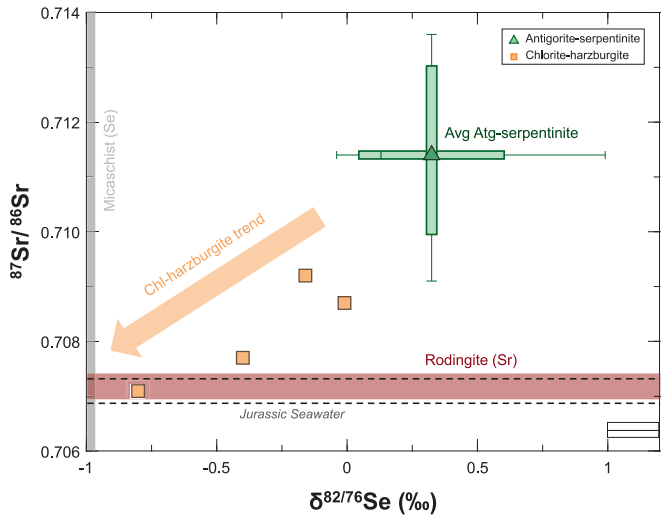

Fig. 5. Selenium vs. strontium isotope compositions of CdA Atg-serpentinites and Chl-harzburgites. Atg-serpentinites are shown as box plots, with a green triangle indicating their average composition. The orange arrow marks the positive correlation observed in Chl-harzburgites. The lower $\delta^{82/76}$Se and $^{87}Sr/^{86}Sr$ values in Chl-harzburgites relative to Atg-serpentinites are explained by the mixing of two components: (i) an unradiogenic, AOC-like Sr contribution from CdA rodingites ($^{87}Sr/^{86}Sr$ = 0.7069–0.7074), overlapping with Jurassic seawater ($^{87}Sr/^{86}Sr$ = 0.7068–0.7073; Wierzbowski et al., 2017); and (ii) a sediment-derived light $\delta^{82/76}$Se contribution similar to NFC micaschists ($\delta^{82/76}Se_{AL96-12a} = -0.98 \pm 0.13$‰). Analytical uncertainty for $\delta^{82/76}$Se is shown in the bottom right; $^{87}Sr/^{86}Sr$ uncertainty is smaller than the symbol size.

eclogite generates large $\delta^{82/76}$Se variability in eclogites ($\delta^{82/76}$Se = −1.89 to + 0.48‰; König et al., 2021), overlapping with the variability observed in CdA Chl-harzburgites and Atg-serpentinites ($\delta^{82/76}$Se = −0.80 to + 0.99‰; Fig. 2a, Fig. 3). During prograde devolatilization at Raspas, multi-stage, fluid-restricted fluxes reworked the Se budget within sulfides under relatively closed-system conditions. The infiltration of oxidizing fluids dissolved pre-existing sulfides, but subsequent interaction with the surrounding slab matrix at variable fluid/rock ratios lowered the fluid oxygen fugacity (fO_2), partially reducing the dissolved Se oxyanions (Se^{VI} or Se^{IV}). This reduction triggered the crystallization of new sulfides that preferentially captured the light Se isotopes, driving the residual fluid toward progressively heavier isotopic compositions. This evolution explains the positive correlation observed between $\delta^{82/76}$Se values and FME/Ce ratios in the Raspas eclogites. Early formed, low $\delta^{82/76}$Se sulfides precipitated from relatively unevolved fluid pulses characterized by modest FME budgets, whereas subsequent sulfides crystallized from evolved, FME-loaded fluids that had systematically shifted toward heavier Se isotopic compositions.

In the CdA ultramafic massif, the covariation of FME/Ce ratios with $\delta^{82/76}$Se defines an overall inverse relationship, in contrast to the positive covariation typical of the Raspas suite (Fig. 3a–c). Moreover, while CdA Atg-serpentinites are rather scattered (Fig. 3a–c), the CdA Chl-harzburgites display a well-defined trend opposite to that of Raspas, with increasing FME/Ce at decreasing Se isotope ratios (Fig. 3d–f). Although these suites represent different lithologies (i.e., mafic eclogites vs ultramafic rocks), the initial budget of Ce or FME does not dictate the slope of these trends, as Ce acts strictly as an immobile denominator to normalize fluid-mediated mass transfer (Debret et al., 2024). Instead, these distinct covariations reflect a fundamental process-related difference between deserpentinization in CdA and redox-induced $\delta^{82/76}$Se fractionation during metamorphic dehydration of the oceanic crust in the Raspas complex. The bimodal $\delta^{82/76}$Se distribution in CdA between isotopically heavy Atg-serpentinites and isotopically light Chl-harzburgites, relative to bulk-rock devolatilization (LOI) and redox ($Fe^{3+}/\Sigma Fe$) proxies (Fig. 4), suggests a potential link between $\delta^{82/76}$Se fractionation and redox variations.

The variations in redox state and fO_2 observed during the transition from CdA Atg-serpentinites to Chl-harzburgites have been attributed to a decrease in the $Fe^{3+}/\Sigma Fe$ ratio driven by fluid loss during prograde dehydration (Debret et al., 2015), changes in local buffering capacities during closed or open-system deserpentinization (Trommsdorff et al., 1998; Padrón-Navarta et al., 2011, 2023), or a pre-subduction oceanic oxidation front that established initial redox heterogeneities (Bretscher et al., 2018; Vieira Duarte et al., 2021; Pettke and Bretscher, 2022). As discussed earlier, lighter Se isotope compositions compared to primitive mantle rule out the pre-subduction oceanic redox front scenario. Instead, this isotopic shift is better explained by a relative decrease in fO_2 driven by deserpentinization (Piccoli et al., 2019; Padrón-Navarta et al., 2023).

Given that significant Se kinetic isotope fractionation requires oxyanion reduction (Johnson, 2004), the redox gradient (Fig. 4) during high-P deserpentinization offers a likely driver for the Se isotopic fractionation. Redox conditions associated with closed-system deserpentinization of fully serpentinized peridotite have been tightly constrained by both experimental studies (e.g., Merkulova et al., 2017; Iacovino et al., 2020; Maurice et al., 2020) and thermodynamic models (e.g., Piccoli et al., 2019; Evans and Frost, 2020), yielding highly debated estimates that range from − 1 to + 4.6 $\Delta \log fO_2$ [FMQ]. The fO_2 conditions determined in CdA and other exhumed metaperidotites record lower values than those determined by these closed-system baselines. This discrepancy has been interpreted by some authors as evidence that closed-system intrinsic deserpentinization is reducing (Piccoli et al., 2019; Evans and Frost, 2020). If sulfide precipitation and Se isotope fractionation were driven by a reducing gradient during closed-system deserpentinization, one would expect positive correlations between FME/Ce and $\delta^{82/76}$Se, as observed in the Raspas Complex. The observed inverse relationship between FME/Ce and $\delta^{82/76}$Se in CdA suite (Fig. 3a–c) and Chl-harzburgites (Fig. 3d–f) makes this scenario unlikely.

Alternatively, thermodynamic modelling of intrinsic deserpentinization (i.e., closed-system) indicates that the generated fluids can become highly oxidizing, evolving near the haematite-magnetite (HM) buffer (Debret and Sverjensky, 2017; Padrón-Navarta et al., 2023). The exact path of this redox evolution depends on the initial redox budget of the rock (Debret and Sverjensky, 2017). However, a closed-system scenario (even when locally buffered by sulfides) remains difficult to reconcile with the overall CdA redox evolution from Atg-serpentinites to Chl-harzburgites. Under highly oxidizing conditions, S and Se should be mobilized as aqueous sulfate species (predominantly HSO_4^- and SO_4^{2-}) and, likely, analogous selenate species ($HSeO_4^-$ and SeO_4^{2-}). This model predicts the complete dissolution of sulfides and the formation of high-Fo olivine, which is at odds with the mineralogical evidence from CdA (Padrón-Navarta et al., 2023). According to experimental and theoretical constraints, the oxidative mobilization of Se induces negligible isotopic fractionation (typically < 0.5‰) (Johnson, 2004; Stüeken et al., 2015). This is because oxidation involves the formation of new Se–O bonds rather than the kinetic rupture of bonds that drives selenium fractionation during reduction (Johnson, 2004). Furthermore, the oxidation of solid reduced phases (e.g., Se^0 or sulfide-bound Se^{-II}) proceeds via surface-layer stripping, a quantitative process that prevents the expression of kinetic isotope fractionation (Johnson, 2004). Consequently, a simple gradient of increasing oxidation during intrinsic deserpentinization would transfer the bulk isotopic composition of the rock into the fluid without $\delta^{82/76}$Se fractionation. This scenario cannot account for the negative FME/Ce vs $\delta^{82/76}$Se trend in the CdA suite (Fig. 3a–c), and particularly, that of the Chl-harzburgite deserpentinization products (Fig. 3d–f).

To reconcile the redox discrepancy in CdA, Padrón-Navarta et al. (2023) proposed that redox conditions during deserpentinization were modulated by the ingress of relatively reducing metasediment-derived fluids. The likely source for these fluids is the co-subducted Carboniferous graphite-micaschists of the Nevado-Filábride Complex (NFC)

(Jabaloy-Sánchez et al., 2015). Metasedimentary lithologies of this type characteristically exhibit elevated FME concentrations coupled with isotopically light selenium ($\delta^{82/76}$Se ≤ -4‰; Stüeken et al., 2015), a signature locally corroborated by the NFC micaschist (sample AL96-12a: $\delta^{82/76}$Se $= -0.98 \pm 0.13$‰; Table S1). This distinct end-member, enriched in FME and characterized by low $\delta^{82/76}$Se, constrains the FME/Ce and Se isotope signature of the infiltrated metasediment-derived fluids.

During deserpentinization modulated by sediment-derived relatively reducing fluids, the oxidation state of the system evolves as a function of the fluid-rock ratio, from highly oxidizing ($\Delta\log fO_2$ FMQ + 3.2) to progressively more reducing ($\Delta\log fO_2$ FMQ + 2.4) (Figs. S5a, b) (Padrón-Navarta et al., 2023). Initially, high-fO_2 intrinsic deserpentinization fluids would dissolve pre-existing sulfides, mobilizing S and Se respectively as hydrogen sulfate (HSO_4^-) and, likely, hydrogen selenate ($HSeO_4^-$) species. Subsequent antigorite dehydration enhances porosity, facilitating the progressive infiltration of the sediment-derived fluids at increasing fluid-rock ratios, establishing a redox gradient that drives sulfide precipitation (Figs. S5c–f; Padrón-Navarta et al., 2023). If selenium isotope fractionation were kinetically controlled by this precipitation in a progressively reducing redox gradient, as in the Raspas Complex (König et al., 2021), CdA Chl-harzburgite with the lowest FME/Ce ratios (indicating low fluid-rock ratios) should record the lowest $\delta^{82/76}$Se. Instead, the CdA Chl-harzburgites display the inverse trend, with samples with lower FME/Ce ratios yielding isotopically heavier Se (Fig. 3d–f). This trend excludes redox-driven fractionation of $\delta^{82/76}$Se as the governing process during deserpentinization modulated by sediment-derived fluids. Thus, while fluid infiltration induces a substantial redox gradient, Se isotopes in the CdA suite primarily record their sediment-fluid provenance rather than local redox-dependent fractionation during high-pressure deserpentinization.

5.3. Sediment- and AOC-derived fluids interaction during deserpentinization

Several geochemical observations in the CdA suite point to fluid mixing during deserpentinization. Specifically, the systematic covariation of $\delta^{82/76}$Se and ^{87}Sr/^{86}Sr in CdA Chl-harzburgites relative to their Atg-serpentinite protoliths provides strong evidence for a multi-component fluid history (Fig. 5). The observed trend implies an infiltrating fluid characterized by isotopically light Se, relatively unradiogenic Sr, and elevated FME/Ce (Fig. S1).

While fluids derived from NFC metasedimentary rocks could account for the elevated FME/Ce ratios and light Se signatures (Figs. 2 and 3), their ^{87}Sr/^{86}Sr values are too radiogenic (e.g., ^{87}Sr/^{86}Sr = 0.7246 in NFC micaschist AL96-12a; Table S1) to generate the trend observed in the CdA Chl-harzburgites (Fig. 5). Although the radiogenic signature of the co-subducted NFC Carboniferous metasediments (Jabaloy-Sánchez et al., 2015) might be attributed to a detrital continental input increasing the original Carboniferous seawater ratio (^{87}Sr/^{86}Sr ≈ 0.7077; Chen et al., 2022), the least radiogenic Chl-harzburgite (^{87}Sr/^{86}Sr = 0.7071; Fig. 5) is even lower than this baseline, rendering a purely sedimentary Sr source unlikely. Conversely, while unradiogenic Sr is typical of AOC-derived slab fluids (Turner and Langmuir, 2022, 2024) and AOC-eclogites can supply light Se (König et al., 2021), such fluids would be too FME-depleted and highly oxidized to produce the combined geochemical and redox signatures of the CdA Chl-harzburgites. This apparent duality of the subduction components is common in arc lavas due to variable contribution of mixed-fluid derived from subducted sediments and AOC (Elliott, 2003; Bebout, 2014; Bebout and Penniston-Dorland, 2016; Ague, 2017; Rustioni et al., 2021; Turner and Langmuir, 2022, 2024).

The positive correlation between isotopically light Se and unradiogenic Sr (Fig. 5) is best explained by the mixing of two complementary fluid components, sediment- and AOC-derived, during deserpentinization. Unlike the scattered Atg-serpentinites, CdA Chl-harzburgites define Sr/Ce vs. ^{87}Sr/^{86}Sr trends pointing toward a Jurassic seawater-like component (^{87}Sr/^{86}Sr ≈ 0.7068–0.7073; Wierzbowski et al., 2017) (Fig. 2b; see also Fig. 5). This unradiogenic endmember is best attributed to epidote-metarodingites within the CdA massif, which are strongly enriched in Sr (up to > 0.1 wt%; Tables S1, S2) and underwent subduction contemporaneously with the host CdA ultramafic rocks (Marchesi et al., 2013; Laborda-López et al., 2018, 2020). During deserpentinization, the destabilization of epidote to pyralspite-bearing assemblages in metarodingites releases Sr-rich (Laborda-López et al., 2018; Laborda-López et al., 2020), unradiogenic fluids (^{87}Sr/^{86}Sr = 0.7069–0.7074; Table S1). While the $\delta^{82/76}$Se of metarodingites is isotopically heavy ($\delta^{82/76}$Se = +0.80 to + 2.09‰; Table S1), they possess low pre-deserpentinization Se contents (22–35 ng·g^{-1}; Tables S1, S2). As a result, they supply the required Sr without perturbing the Se budget and $\delta^{82/76}$Se isotopic composition of the fluid. In contrast, the isotopically light Se signature is derived from the NFC micaschists (e.g., $\delta^{82/76}$Se ≈ −0.98‰; Table S1). Although the analyzed NFC micaschists are now Se-poor (44–122 ng·g^{-1}; Table S2), their pre-metamorphic black-shale protoliths were enriched in Se (characteristic Se content of Carboniferous black shales ranges from 600 to > 20,000 ng·g^{-1}; Kipp et al., 2020), implying substantial Se mobilization during prograde metamorphic dehydration of NFC micaschist, especially at conditions of Atg-breakdown in associated serpentinites. While NFC micaschists also contain appreciable Sr (110–132 μg·g^{-1}; Table S2), this element is largely retained within epidote, which remains stable in the NFC micaschists over the relevant metamorphic interval (Gómez-Pugnaire et al., 2019), thereby limiting Sr transfer to the fluid. The geochemical evolution of the CdA Chl-harzburgites documents a physical interaction where subarc deserpentinization fluids are geochemically shaped by the mixing of distinct slab end members, as sketched in Fig. 6.

In this open-system scenario (Fig. 6), external fluids released from the dehydration of co-subducted metasediments infiltrated the dehydrating serpentinite slab section, as proposed by Padrón-Navarta et al. (2023). These infiltrating fluids carried the sedimentary subduction component characterized by high FME abundances and an isotopically light Se signature acquired from their black shale protoliths. As these fluids percolated through the deserpentinization front, they interacted with metarodingites (embedded remnants of the mafic intrusions) which were simultaneously undergoing high-pressure breakdown from epidote to pyralspite-bearing assemblages (Laborda-López et al., 2018). This reaction liberated the AOC-like Sr component stored in the destabilizing epidote. The $\delta^{82/76}$Se versus ^{87}Sr/^{86}Sr positive correlation in CdA Chl-harzburgites (Fig. 5) records the sediment–oceanic crust fluid interaction during slab deserpentinization, with the external sedimentary fluid supplying the light Se, and the internal reacting rodingites supplying the unradiogenic Sr (Fig. 5). Deserpentinization acts as a mixing engine, integrating disparate sedimentary and crustal signatures into a unified slab fluid flux (Fig. 6) that ultimately shapes the subduction component recycled into the mantle wedge that sources arc volcanism (Bebout, 2014; Bebout and Penniston-Dorland, 2016; Ague, 2017; Rustioni et al., 2021; Turner and Langmuir, 2022, 2024).

5.4. Modelling of sediment–oceanic crust interaction modulated by open-system deserpentinization

To investigate the selenium and strontium geochemical evolution during deserpentinization, we developed an open-system deserpentinization (OSD) numerical model adapted from the analytical solutions for open-system melting from Ozawa (2001). Model details and equations are provided in section C in the Supplementary Information. Following the conceptual framework in Fig. 6, the model simulates the infiltration of a metasediment-equilibrated fluid into a heterogeneous deserpentinizing slab containing AOC-like metarodingite heterogeneities. The metasediment-equilibrated fluid is calculated as a fluid in equilibrium with a NFC micaschist. The resulting fluid has a relatively high Se/Sr

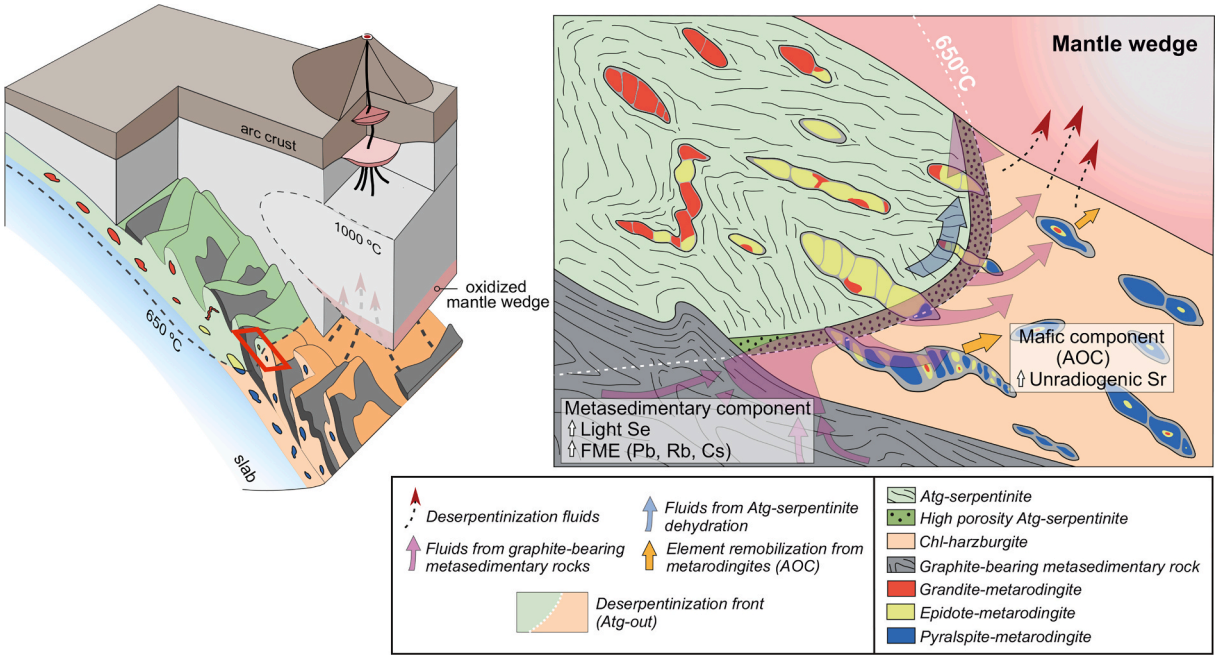

Fig. 6. Conceptual model illustrating open-system deserpentinization-driven fluid–rock interaction and the mixing of distinct slab components. External fluids derived from co-subducted graphite-bearing metasediments (pink arrows) infiltrate the dehydrating Atg-serpentinite (blue arrow), introducing a sedimentary signature characterized by high Fluid Mobile Element (FME) concentrations and isotopically light Selenium. As these fluids infiltrate the deserpentinization front, they interact with embedded metarodingites (AOC), which simultaneously release unradiogenic Strontium due to the metamorphic breakdown of epidote. The resulting Chl-harzburgites thus record the integration of two complementary sources: an external, light Se metasedimentary-derived fluid and the metarodingite unradiogenic Sr contribution (cartoons modified from Padrón-Navarta et al., 2023, and Laborda-López et al., 2020).

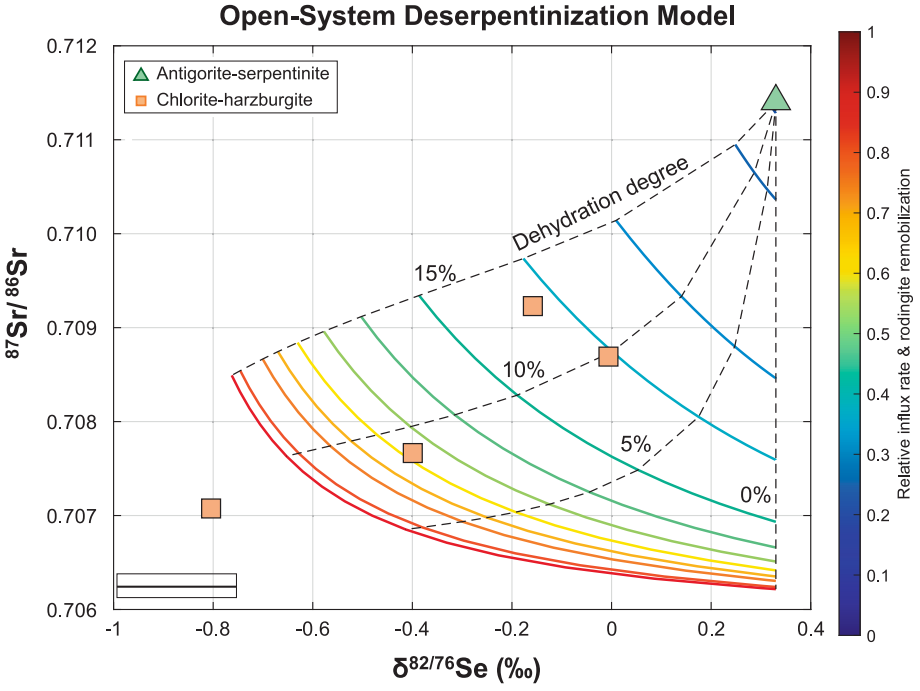

Fig. 7. Trajectories of $\delta^{82/76}$Se–^{87}Sr/^{86}Sr predicted by the OSD model for the isotopic composition of prograde metaharzburgite formed by open-system dehydration of Atg-serpentinite, with metarodingite heterogeneities, infiltrated by metasediment-derived fluids. The composition of the serpentinite protolith is represented by the average Cerro del Almirez Atg-serpentinite (green closed triangle) (see Fig. 5). The short-dashed lines are isocontours of relative mass loss due to dehydration, f, ranging from 0 to 15% in 5% intervals (see Supplementary Material for further details), where ca. 10% mass loss corresponds to complete Atg-dehydration (Padrón-Navarta et al., 2023). Also shown in colour are β isocontours, where β is the relative metasediment-derived fluid influx and the metarodingite–Atg-serpentinite elemental redistribution (see Supplementary Material for further details). Note that $\delta^{82/76}$Se–^{87}Sr/^{86}Sr trends of the Cerro del Almirez Chl-harzburgite (orange squares) are better explained for $f \approx 10\%$ (in the range of complete dehydration) at increasing β values, i.e., at increasing metasediment-derived fluid influx and Atg-serpentinite–metarodingite elemental redistribution. Analytical uncertainty for $\delta^{82/76}$Se is shown in the bottom left; ^{87}Sr/^{86}Sr uncertainty is smaller than the symbol size.

because Sr is strongly retained in epidote (high epidote–fluid partition coefficient for Sr), limiting transfer of Sr from micaschist to the fluid. The bulk reacting serpentinite composition is calculated by mass balance between an average CdA Atg-serpentinite and 5 wt% metarodingite, corresponding to the average abundance of metarodingite in the Cerro del Almirez (Laborda-López et al., 2018). The element transfer between metarodingite and serpentinite scales with the relative metasediment-derived fluid influx rate (β) (see section C in the Supplementary Information).

The trajectories of $\delta^{82/76}$Se – ^{87}Sr/^{86}Sr predicted by the best-fit OSD model are shown in Fig. 7. The observed positive $\delta^{82/76}$Se – ^{87}Sr/^{86}Sr trend in CdA Chl-harzburgites is best reproduced for $f \approx 10\%$, where f is the relative mass loss due to dehydration (ca. 10% mass loss corresponding to complete Atg-serpentinite dehydration; Padrón-Navarta et al., 2023), together with progressively increasing β. Relative to their Atg-serpentinite protoliths, increasing β drives the modelled compositions of Chl-harzburgite toward isotopically lighter Se (i.e., lower $\delta^{82/76}$Se) and more unradiogenic Sr (lower ^{87}Sr/^{86}Sr) (Fig. 7), consistent with progressively greater influx of metasediment-derived fluid and increasing Sr contribution from epidote-metarodingite.

Although the model does not explicitly calculate the FME/Ce relations, the observed covariations of FME/Ce and Sr/Ce with ^{87}Sr/^{86}Sr (Fig. 2b; Figs. S1a–c) are consistent with the same increase in β. Metarodingite increasing contribution dominates the Sr budget and imposes the unradiogenic ^{87}Sr/^{86}Sr signature, whereas metasediment-derived fluids supply FME and isotopically light Se.

6. Conclusions

Arc magmas acquire their subduction signature from fluids generated within structurally heterogeneous slabs, where serpentinite, metasediments, and altered oceanic crust interact during deserpentinization. At Cerro del Almirez, systematic differences in Se–Sr isotopes, FME contents, $Fe^{3+}/\Sigma Fe$, and LOI between Atg-serpentinites and Chl-harzburgites cannot be explained by magmatic inheritance, variable seafloor serpentinization, or closed-system devolatilization alone; they require infiltration of externally sourced fluids and interaction with internal slab heterogeneities.

The negative covariation between $\delta^{82/76}$Se and FME/Ce observed in Chl-harzburgites, formed after an Atg-serpentinite protolith, together with the bimodal Se isotope distribution and redox proxies, argues against redox-controlled Se isotope fractionation during deserpentinization and instead shows that Se isotopes primarily track an external metasediment fluid source. Selenium and Sr isotope systematics indicate that Chl-harzburgites reflect the combined and coeval effects of (i) Atg-serpentine dehydration, (ii) influx of isotopically-light Se, FME-rich fluids derived from co-subducted metasediments, and (iii) addition of AOC-like unradiogenic Sr released from epidote-metarodingite boudins interspersed in Atg-serpentinites. An open-system deserpentinization model reproduces the $\delta^{82/76}$Se – ^{87}Sr/^{86}Sr trends for near-complete antigorite dehydration and progressively increasing fluxes of metasediment-equilibrated fluids interacting with a serpentinite–rodingite assemblage.

These results show that, in compositionally heterogeneous slabs, reactive infiltration during deserpentinization can transfer sediment-derived Se–FME signatures and AOC-derived Sr signatures into the same fluid flux before release to the mantle wedge, thereby modulating the apparent sediment–AOC proportions recorded by the subduction-zone fluid component of primitive arc magmas. Beyond the Cerro del Almirez massif, the lithological configuration examined here, hydrated slab mantle hosting mafic intrusions rodingitized during seafloor hydrothermal metasomatism, is a widespread feature of oceanic lithosphere generated at slow and ultraslow spreading ridges. Deserpentinization driven mixing between sediment derived Se-FME signatures and AOC derived Sr signatures is therefore expected to operate as a general subarc process shaping the subduction component of arc magmatism wherever such heterogeneous slab mantle serpentinites are co subducted with metasediments. Analogous sediment–AOC coupling may additionally develop at shallower forearc depths in slab interface mélange zones, where the same lithological end members interact by different mechanisms (Bebout, 2007).

Data availability

Data are available through DIGITAL.CSIC at https://doi.org/10.20350/digitalCSIC/17876.

Declaration of generative AI and AI-assisted technologies in the manuscript preparation process

During the preparation of this work, the authors used Gemini, Copilot, and ChatGPT in order to search for information, synthesize and restructure ideas, verify logical coherence, and improve language and readability. After using these tools, the authors reviewed and edited the content as needed and took full responsibility for the final content of the published article.

CRediT authorship contribution statement

Juan Muñoz-Alfaro: Writing – review & editing, Writing – original draft, Visualization, Project administration, Methodology, Investigation, Formal analysis, Data curation, Conceptualization. **Stephan König:** Writing – review & editing, Validation, Supervision, Resources, Methodology, Investigation, Funding acquisition, Formal analysis. **Claudio Marchesi:** Writing – review & editing, Validation, Resources, Methodology, Investigation, Formal analysis, Data curation, Conceptualization. **Romain Tilhac:** Writing – review & editing, Visualization, Validation, Software, Formal analysis. **María Isabel Varas-Reus:** Writing – review & editing, Methodology. **José Alberto Padrón-Navarta:** Writing – review & editing, Validation, Resources, Funding acquisition. **Vicente López Sánchez-Vizcaíno:** Writing – review & editing, Resources, Investigation, Funding acquisition. **Ronny Schoenberg:** Writing – review & editing, Resources. **Carlos J. Garrido:** Writing – review & editing, Writing – original draft, Visualization, Validation, Supervision, Resources, Project administration, Methodology, Investigation, Funding acquisition, Formal analysis, Conceptualization.

Declaration of competing interest

The authors declare that they have no known competing financial interests or personal relationships that could have appeared to influence the work reported in this paper.

Acknowledgements

We thank Marianne Richter for her help with Sr isotope measurements, and Elmer Reitter (Tuebingen), Diana Lara-García, Deyanira Rondón-Rodríguez, and Manuel Jesús Román-Alpiste (Granada) for their assistance during clean-lab procedures and instrumental analysis. We also thank Casto Laborda-López for his contribution to the fieldwork and sampling of the metarodingite samples.

Selenium isotopes analyses in CdA were initiated with funding from ERC-STG-2014 (636808, O2RIGIN) to S. König, and a two-month research stay by C. Marchesi at the University of Tuebingen funded the University of Granada “Plan Propio de Investigación 2018 – Short Research Stays in Foreign Institutions”. S. König also acknowledges funding from project PROYEXCEL_00848 and RYC2020-030014-1. J. Muñoz-Alfaro, C.J. Garrido, J.A. Padrón-Navarta, and V. López Sánchez-Vizcaíno acknowledge funding from projects PID2022-136471NB-C21&C22 (RUSTED) funded by MCIN/AEI/10.13039/501100011033 and co-funded by the European Union (ERDF—A way of making Europe). R. Tilhac acknowledges funding from fellowship IJC2020-

044739-I (Juan de la Cierva-Incorporación). J. Muñoz-Alfaro acknowledges fellowship PREDOC_00939 by Junta de Andalucía and European Union ("Andalucía se mueve con Europa").

Appendix A. Supplementary material

This article includes three Supplementary Materials. Supplementary Information provides a detailed description of the methodology used for Selenium and Strontium analyses (section A), along with the complete models' specifications and equations (sections B and C). It also contains the Supplementary Figures referenced in the main text. Additionally, Supplementary Data 1 includes Tables S1 and S2, which present our $\delta^{82}/^{76}$Se and $^{87}Sr/^{86}Sr$ results, as well as additional data relevant to this study. Finally, Supplementary Data 2 includes the calculations of the Rayleigh distillation modelling for equilibrium Se isotope fractionation, which is further described and illustrated in Figure S4 (Supplementary Information).

Supplementary material to this article can be found online at https://doi.org/10.1016/j.gca.2026.07.049.

References

Ague, J.J., 2017. Element mobility during regional metamorphism in crustal and subduction zone environments with a focus on the rare earth elements (REE). Am. Mineral. 102, 1796–1821.
Ague, J.J., Tassara, S., Holycross, M.E., Li, J.-L., Cottrell, E., Schwarzenbach, E.M., Fassoulas, C., John, T., 2022. Slab-derived devolatilization fluids oxidized by subducted metasedimentary rocks. Nat. Geosci. 15, 320–326.
Alt, J.C., Garrido, C.J., Shanks, W.C., Turchyn, A., Padrón-Navarta, J.A., López, S.-V., Gómez-Pugnaire, M.T., Marchesi, C., 2012. Recycling of water, carbon, and sulfur during subduction of serpentinites: a stable isotope study of Cerro del Almirez. Spain. Earth Planet. Sci. Lett. 327–328, 50–60.
Alt, J.C., Schwarzenbach, E.M., Früh-Green, G.L., Shanks, W.C., Bernasconi, S.M., Garrido, C.J., Crispini, L., Gaggero, L., Padrón-Navarta, J.A., Marchesi, C., 2013. The role of serpentinites in cycling of carbon and sulfur: seafloor serpentinization and subduction metamorphism. Lithos 178, 40–54.
Bebout, G.E., 2007. Metamorphic chemical geodynamics of subduction zones. Earth Planet. Sci. Lett. 260, 373–393.
Bebout, G.E., 2014. Chemical and isotopic cycling in subduction zones. In: Holland, H.D., Turekian, K.K. (Eds.), Treatise on Geochemistry, Second ed. Elsevier, Oxford, pp. 703–747.
Bebout, G.E., Penniston-Dorland, S.C., 2016. Fluid and mass transfer at subduction interfaces—the field metamorphic record. Lithos 240, 228–258.
Bretscher, A., Hermann, J., Pettke, T., 2018. The influence of oceanic oxidation on serpentinite dehydration during subduction. Earth Planet. Sci. Lett. 499, 173–184.
Cerpa, N.G., Arcay, D., Padrón-Navarta, J.A., 2022. Sea-level stability over geological time owing to limited deep subduction of hydrated mantle. Nat. Geosci. 15, 423–428.
Chang, Y., Zhang, J., Qu, J.-Q., Xue, Y., 2017. Precise selenium isotope measurement in seawater by carbon-containing hydride generation-desolvation-MC-ICP-MS after thiol resin preconcentration. Chem. Geol. 471, 65–73.
Chen, J., Chen, B., Montañez, I.P., 2022. Carboniferous isotope stratigraphy. Geol. Soc. Lond. Spec. Publ. 512, 655–691.
Chen, L., Li, D.-Y., Deng, J.-H., Li, S.-Z., Somerville, I., Chen, Y.-X., Zhao, Z.-F., An, W., Li, X.-H., 2023. Fe–Mg isotopes trace the mechanism of crustal recycling and arc magmatic processes in the Neo-Tethys subduction Zone. J. Geophys. Res. Solid Earth 128, e2023JB026778.
Chen, S., Hin, R.C., John, T., Brooker, R., Bryan, B., Niu, Y., Elliott, T., 2019. Molybdenum systematics of subducted crust record reactive fluid flow from underlying slab serpentine dehydration. Nat. Commun. 10, 4773.
Connolly, J.A.D., 1997. Devolatilization-generated fluid pressure and deformation-propagated fluid flow during prograde regional metamorphism. J. Geophys. Res. Solid Earth 102, 18149–18173.
Debret, B., Sverjensky, D.A., 2017. Highly oxidising fluids generated during serpentinite breakdown in subduction zones. Sci. Rep. 7, 10351.
Debret, B., Bolfan-Casanova, N., Padrón-Navarta, J.A., Martin-Hernandez, F., Andreani, M., Garrido, C.J., López, S.-V., Gómez-Pugnaire, M.T., Muñoz, M., Trcera, N., 2015. Redox state of iron during high-pressure serpentinite dehydration. Contrib. Miner. Petrol. 169, 1–18.
Debret, B., Caurant, C., Ménez, B., Busigny, V., Moynier, F., 2024. Evidence for isotopically light Fe mobility under oxidising conditions in subduction zone fluids: a record of Monviso meta-serpentinites. Western Alps. Earth Planet. Sci. Lett. 642, 118855.
Debret, B., Garrido, C.J., Pons, M.-L., Bouilhol, P., Inglis, E., López, S.-V., Williams, H., 2021. Iron and zinc stable isotope evidence for open-system high-pressure dehydration of antigorite serpentinite in subduction zones. Geochim. Cosmochim. Acta 296, 210–225.
Debret, B., Millet, M.-A., Pons, M.-L., Bouilhol, P., Inglis, E., Williams, H., 2016. Isotopic evidence for iron mobility during subduction. Geology 44, 215–218.
Dilissen, N., Hidas, K., Garrido, C.J., Kahl, W.-A., López, S.-V., Padrón-Navarta, J.A., 2018. Textural evolution during high-pressure dehydration of serpentinite to peridotite and its relation to stress orientations and kinematics of subducting slabs: insights from the Almirez ultramafic massif. Lithos 320–321, 470–489.
Elliott, T., 2003. Tracers of the slab. Geophys. Monogr. Ser. 138, 23–46.
Evans, K.A., Frost, B.R., 2020. Deserpentinization in subduction zones as a source of oxidation in arcs: a reality check. J. Petrol. 62, 1–32.
Garrido, C.J., López, S.-V., Gómez-Pugnaire, M.T., Trommsdorff, V., Alard, O., Bodinier, J.-L., Godard, M., 2005. Enrichment of HFSE in chlorite-harzburgite produced by high-pressure dehydration of antigorite-serpentinite: implications for subduction magmatism. Geochem. Geophys, Geosystems, p. 6.
Gómez-Pugnaire, M.T., Nieto, F., Abad, I., Velilla, N., Garrido, C.J., Acosta-Vigil, A., Barich, A., Hidas, K., López Sánchez-Vizcaíno, V., 2019. Alpine metamorphism in the Betic Internal Zones. In: Quesada, C., Oliveira, J.T. (Eds.), The Geology of Iberia: A Geodynamic Approach, Volume 3: The Alpine Cycle. Springer, Cham, pp. 519–544.
Halama, R., Bebout, G.E., John, T., Scambelluri, M., 2014. Nitrogen recycling in subducted mantle rocks and implications for the global nitrogen cycle. Int. J. Earth Sci. 103, 2081–2099.
Harvey, J., Garrido, C.J., Savov, I., Agostini, S., Padrón-Navarta, J.A., Marchesi, C., López, S.-V., Gómez-Pugnaire, M.T., 2014. 11B-rich fluids in subduction zones: the role of antigorite dehydration in subducting slabs and boron isotope heterogeneity in the mantle. Chem. Geol. 376, 20–30.
Hirschmann, M.M., 2023. The deep Earth oxygen cycle: mass balance considerations on the origin and evolution of mantle and surface oxidative reservoirs. Earth Planet. Sci. Lett. 619, 118311.
Hochscheid, F., Coltat, R., Ulrich, M., Munoz, M., Manatschal, G., Boulvais, P., 2022. The Sr isotope geochemistry of oceanic ultramafic-hosted mineralizations. Ore Geol. Rev. 144, 104824.
Iacovino, K., Guild, M.R., Till, C.B., 2020. Aqueous fluids are effective oxidizing agents of the mantle in subduction zones. Contrib. Miner. Petrol. 175, 36.
Jabaloy-Sánchez, A., Gómez-Pugnaire, M.T., Padrón-Navarta, J.A., López, S.-V., Garrido, C.J., 2015. Subduction- and exhumation-related structures preserved in metaserpentinites and associated metasediments from the nevado-filábride complex (Betic Cordillera, SE Spain). Tectonophysics 644, 40–57.
Jabaloy-Sánchez, A., Padrón-Navarta, J.A., Gómez-Pugnaire, M.T., López Sánchez-Vizcaíno, V., Garrido, C.J., 2019. Alpine Orogeny: Deformation and Structure in the Southern Iberian Margin (Betics s.l.). In: Quesada, C., Oliveira, J.T. (Eds.), The Geology of Iberia: A Geodynamic Approach, Volume 3: The Alpine Cycle. Springer, Cham, pp. 453–486.
John, T., Gussone, N., Podladchikov, Y.Y., Bebout, G.E., Dohmen, R., Halama, R., Klemd, R., Magna, T., Seitz, H.-M., 2012. Volcanic arcs fed by rapid pulsed fluid flow through subducting slabs. Nat. Geosci. 5, 489–492.
John, T., Klemd, R., Gao, J., Garbe-Schönberg, C.-D., 2008. Trace-element mobilization in slabs due to non steady-state fluid–rock interaction: constraints from an eclogite-facies transport vein in blueschist (Tianshan, China). Lithos 103, 1–24.
Johnson, T.M., 2004. A review of mass-dependent fractionation of selenium isotopes and implications for other heavy stable isotopes. Chem. Geol. 204, 201–214.
Kendrick, M.A., Scambelluri, M., Hermann, J., Padrón-Navarta, J.A., 2018. Halogens and noble gases in serpentinites and secondary peridotites: implications for seawater subduction and the origin of mantle neon. Geochim. Cosmochim. Acta 235, 285–304.
Kessel, R., Schmidt, M.W., Ulmer, P., Pettke, T., 2005. Trace element signature of subduction-zone fluids, melts and supercritical liquids at 120–180 km depth. Nature 437, 724–727.
Kipp, M.A., Algeo, T.J., Stüeken, E.E., Buick, R., 2020. Basinal hydrographic and redox controls on selenium enrichment and isotopic composition in Paleozoic black shales. Geochim. Cosmochim. Acta 287, 229–250.
Kochergina, Y.V.E., Erban, V., Hora, J.M., 2022. Sample preparation and chromatographic separation for Sr, Nd, and Pb isotope analysis in geological, environmental, and archaeological samples. J. Geosci. 67, 259–271.
König, S., Eickmann, B., Zack, T., Yierpan, A., Wille, M., Taubald, H., Schoenberg, R., 2019. Redox induced sulfur-selenium isotope decoupling recorded in pyrite. Geochim. Cosmochim. Acta 244, 24–39.
König, S., Rosca, C., Kurzawa, T., Varas-Reus, M.I., Dragovic, B., Schoenberg, R., John, T., 2021. Selenium isotope evidence for pulsed flow of oxidative slab fluids. Geochem. Perspect. Lett. 17, 27–32.
Kurzawa, T., König, S., Alt, J.C., Yierpan, A., Schoenberg, R., 2019. The role of subduction recycling on the selenium isotope signature of the mantle: constraints from Mariana arc lavas. Chem. Geol. 513, 239–249.
Kurzawa, T., König, S., Labidi, J., Yierpan, A., Schoenberg, R., 2017. A method for Se isotope analysis of low ng-level geological samples via double spike and hydride generation MC-ICP-MS. Chem. Geol. 466, 219–228.
Laborda-López, C., López Sánchez-Vizcaíno, V., Marchesi, C., Gómez-Pugnaire, M.T., Garrido, C.J., Jabaloy-Sánchez, A., Padrón-Navarta, J.A., Hidas, K., 2018. High-P metamorphism of rodingites during serpentinite dehydration (Cerro Almirez, Southern Spain): Implications for the redox state in subduction zones. J. Metamorph. Geol. 36 (6), 741–773.
Laborda-López, C., Marchesi, C., López, S.-V., Gómez-Pugnaire, M.T., Dale, C.W., Jabaloy-Sánchez, A., Padrón-Navarta, J.A., Román-Alpiste, M.J., Garrido, C.J., 2020. Geochemical evolution of rodingites during subduction: insights from Cerro del Almirez (southern Spain). Lithos 370–371.
Li, X., Liu, Y., 2011. Equilibrium Se isotope fractionation parameters: a first-principles study. Earth Planet. Sci. Lett. 304, 113–120.
Marchesi, C., Garrido, C.J., Padrón-Navarta, J.A., López, S.-V., Gómez-Pugnaire, M.T., 2013. Element mobility from seafloor serpentinization to high-pressure dehydration

of antigorite in subducted serpentinite: insights from the Cerro del Almirez ultramafic massif (southern Spain). Lithos 178, 128–142.
Martínez-Martínez, J.M., Soto, J.I., Balanyá, J.C., 2002. Orthogonal folding of extensional detachments: structure and origin of the Sierra Nevada elongated dome (Betics, SE Spain). Tectonics 21, 3-1-3–20.
Maurice, J., Bolfan-Casanova, N., Demouchy, S., Chauvigne, P., Schiavi, F., Debret, B., 2020. The intrinsic nature of antigorite breakdown at 3 GPa: experimental constraints on redox conditions of serpentinite dehydration in subduction zones. Contrib. Miner. Petrol. 175, 94.
Merkulova, M.V., Muñoz, M., Brunet, F., Vidal, O., Hattori, K., Vantelon, D., Trcera, N., Huthwelker, T., 2017. Experimental insight into redox transfer by iron-and sulfur-bearing serpentinite dehydration in subduction zones. Earth Planet. Sci. Lett. 479, 133–143.
O'Neill, H.S.C., Rubie, D.C., Canil, D., Geiger, C.A., Ross, C.R., Seifert, F., Woodland, A. B., 1993. Ferric iron in the upper mantle and in transition zone assemblages: implications for relative oxygen fugacities in the mantle. Evol. Earth Planets 74, 73–88.
Ozawa, K., 2001. Mass balance equations for open magmatic systems: trace element behavior and its application to open system melting in the upper mantle. J. Geophys. Res. Solid Earth 106, 13407–13434.
Padrón-Navarta, J.A., Hermann, J., Garrido, C.J., López, S.-V., Gómez-Pugnaire, M.T., 2010a. An experimental investigation of antigorite dehydration in natural silica-enriched serpentinite. Contrib. Miner. Petrol. 159, 25–42.
Padrón-Navarta, J.A., López, S.-V., Garrido, C.J., Gómez-Pugnaire, M.T., 2011. Metamorphic record of high-pressure dehydration of antigorite serpentinite to chlorite harzburgite in a subduction setting (Cerro del Almirez, Nevado-Filábride complex, Southern Spain). J. Petrol. 52, 2047–2078.
Padrón-Navarta, J.A., López, S.-V., Menzel, M.D., Gómez-Pugnaire, M.T., Garrido, C.J., 2023. Mantle wedge oxidation from deserpentinization modulated by sediment-derived fluids. Nat. Geosci. 16, 268–275.
Padrón-Navarta, J.A., Tommasi, A., Garrido, C.J., Mainprice, D., 2015. On topotaxy and compaction during antigorite and chlorite dehydration: an experimental and natural study. Contrib. Mineral, Petrol, p. 169.
Padrón-Navarta, J.A., Tommasi, A., Garrido, C.J., López, S.-V., Gómez-Pugnaire, M.T., Jabaloy, A., Vauchez, A., 2010b. Fluid transfer into the wedge controlled by high-pressure hydrofracturing in the cold top-slab mantle. Earth Planet. Sci. Lett. 297, 271–286.
Pettke, T., Bretscher, A., 2022. Fluid-mediated element cycling in subducted oceanic lithosphere: the orogenic serpentinite perspective. Earth-Sci, Rev, p. 225.
Piccoli, F., Hermann, J., Pettke, T., Connolly, J.A.D., Kempf, E.D., Vieira Duarte, J.F., 2019. Subducting serpentinites release reduced, not oxidized, aqueous fluids. Sci. Rep. 9, 19573.
Plank, T., 2014. The Chemical Composition of Subducting Sediments. In: Holland, H.D., Turekian, K.K. (Eds.), Treatise on Geochemistry, Second ed. Elsevier, Oxford, pp. 607–629.
Plümper, O., John, T., Podladchikov, Y.Y., Vrijmoed, J.C., Scambelluri, M., 2017. Fluid escape from subduction zones controlled by channel-forming reactive porosity. Nat. Geosci. 10, 150–156.
Puga, E., Nieto, J.M., de Federico, A.D., Bodinier, J., Morten, L., 1999. Petrology and metamorphic evolution of ultramafic rocks and dolerite dykes of the betic ophiolitic association (Mulhacén complex, SE Spain): evidence of eo-Alpine subduction following an ocean-floor metasomatic process. Lithos 49, 23–56.
Rouxel, O., Galy, A., Elderfield, H., 2006. Germanium isotopic variations in igneous rocks and marine sediments. Geochim. Cosmochim. Acta 70, 3387–3400.
Rustioni, G., Audetat, A., Keppler, H., 2021. The composition of subduction zone fluids and the origin of the trace element enrichment in arc magmas. Contrib. Miner. Petrol. 176, 51.
Scambelluri, M., Cannaò, E., Gilio, M., 2019. The water and fluid-mobile element cycles during serpentinite subduction. A Review. Eur. J. Mineral. 31, 405–428.
Scambelluri, M., Tonarini, S., 2012. Boron isotope evidence for shallow fluid transfer across subduction zones by serpentinized mantle. Geology 40, 907–910.
Schmidt, M.W., Poli, S., 2014. Devolatilization During Subduction. In: Holland, H.D., Turekian, K.K. (Eds.), Treatise on Geochemistry, Second ed. Elsevier, Oxford, pp. 669–701.
Schmidt, M.W., Poli, S., 1998. Experimentally based water budgets for dehydrating slabs and consequences for arc magma generation. Earth Planet. Sci. Lett. 163, 361–379.
Snow, J.E., Hart, S.R., Dick, H.J., 1993. Orphan strontium-87 in abyssal peridotites: daddy was a granite. Science 262, 1861–1863.
Stüeken, E.E., 2017. Selenium isotopes as a biogeochemical proxy in deep time. Rev. Mineral. Geochem. 82, 657–682.
Stüeken, E.E., Buick, R., Bekker, A., Catling, D., Foriel, J., Guy, B.M., Kah, L.C., Machel, H.G., Montañez, I.P., Poulton, S.W., 2015. The evolution of the global selenium cycle: secular trends in Se isotopes and abundances. Geochim. Cosmochim. Acta 162, 109–125.
Trommsdorff, V., López, S.-V., Gómez-Pugnaire, M.T., Müntener, O., 1998. High pressure breakdown of antigorite to spinifex-textured olivine and orthopyroxene, SE Spain. Contrib. Miner. Petrol. 132, 139–148.
Turner, S.J., Langmuir, C.H., 2022. Sediment and ocean crust both melt at subduction zones. Earth Planet. Sci. Lett. 584, 117424.
Turner, S.J., Langmuir, C.H., 2024. An alternative to the igneous crust fluid+ sediment melt paradigm for arc lava geochemistry. Sci. Adv. 10, eadg6482.
Ulmer, P., Trommsdorff, V., 1995. Serpentine stability to mantle depths and subduction-related magmatism. Science 268, 858–861.
Varas-Reus, M.I., König, S., Yierpan, A., Lorand, J.-P., Schoenberg, R., 2019. Selenium isotopes as tracers of a late volatile contribution to Earth from the outer Solar System. Nat. Geosci. 12, 779–782.
Vieira Duarte, J.F., Piccoli, F., Pettke, T., Hermann, J., 2021. Textural and geochemical evidence for magnetite production upon antigorite breakdown during subduction. J. Petrol. 62, egab053.
Villa, I.M., De Bièvre, P., Holden, N.E., Renne, P.R., 2015. IUPAC-IUGS recommendation on the half life of 87Rb. Geochim. Cosmochim. Acta 164, 382–385.
Weis, D., Kieffer, B., Maerschalk, C., Barling, J., De Jong, J., Williams, G.A., Hanano, D., Pretorius, W., Mattielli, N., Scoates, J.S., 2006. High-precision isotopic characterization of USGS reference materials by TIMS and MC-ICP-MS. Geochem. Geophys, Geosystems, p. 7.
Whitney, D.L., Evans, B.W., 2010. Abbreviations for names of rock-forming minerals. Am. Mineral. 95, 185–187.
Wierzbowski, H., Anczkiewicz, R., Pawlak, J., Rogov, M.A., Kuznetsov, A.B., 2017. Revised middle–upper Jurassic strontium isotope stratigraphy. Chem. Geol. 466, 239–255.
Xiong, J.-W., Chen, Y.-X., Shen, J., Marchesi, C., Scambelluri, M., Qin, L.-P., López, S.-V., Padrón-Navarta, J.A., Menzel, M.D., Garrido, C.J., 2023. Chromium isotope behavior during serpentinite dehydration in oceanic subduction zones. J. Geophys. Res, Solid Earth, p. 128.
Yang, L., Peter, C., Panne, U., Sturgeon, R.E., 2008. Use of Zr for mass bias correction in strontium isotope ratio determinations using MC-ICP-MS. J. Anal. At. Spectrom 23, 1269–1274.
Yang, Y.-H., Wu, F.-Y., Xie, L.-W., Chu, Z.-Y., Yang, J.-H., 2014. Re-evaluation of interferences of doubly charged ions of heavy rare earth elements on Sr isotopic analysis using multi-collector inductively coupled plasma mass spectrometry. Spectrochim. Acta Part B at. Spectrosc. 97, 118–123.
Yierpan, A., König, S., Labidi, J., Kurzawa, T., Babechuk, M.G., Schoenberg, R., 2018. Chemical sample processing for combined selenium isotope and selenium-tellurium elemental investigation of the Earth's igneous reservoirs. Geochem. Geophys. Geosystems 19, 516–533.
Yierpan, A., König, S., Labidi, J., Schoenberg, R., 2020. Recycled selenium in hot spot–influenced lavas records ocean-atmosphere oxygenation. Sci. Adv. 6, eabb6179.
Yierpan, A., Redlinger, J., König, S., 2021. Selenium and tellurium in Reykjanes Ridge and Icelandic basalts: evidence for degassing-induced Se isotope fractionation. Geochim. Cosmochim. Acta 313, 155–172.
Zack, T., John, T., 2007. An evaluation of reactive fluid flow and trace element mobility in subducting slabs. Chem. Geol. 239, 199–216.
Zindler, A., Hart, S., 1986. Chemical geodynamics. Annu. Rev. Earth Planet. Sci. 14, 493–571.